ELSEVIER

CrossMark

BRACHYTHERAPY

Brachytherapy 22 (2023) 269–278

Treatment verification in high dose rate brachytherapy using a realistic 3D printed head phantom and an imaging panel

Teun van Wagenberg[1,#], Gabriel Paiva Fonseca[1,#], Robert Voncken[1], Celine van Beveren[1], Evert van Limbergen[1], Ludy Lutgens[1], Ben G.L. Vanneste[1,2], Maaike Berbee[1], Brigitte Reniers[3], Frank Verhaegen[1,*]

[1] *Department of Radiation Oncology (Maastro), GROW School for Oncology and Reproduction, Maastricht University Medical Centre+, Maastricht, The Netherlands*

[2] *Department of Human Structure and Repair; Department of Radiation Oncology, Ghent University Hospital, Gent, Belgium*

[3] *Research group NuTeC, Centre for Environmental Sciences, Hasselt University, Diepenbeek, Belgium*

ABSTRACT

PURPOSE: Even though High Dose Rate (HDR) brachytherapy has good treatment outcomes in different treatment sites, treatment verification is far from widely implemented because of a lack of easily available solutions. Previously it has been shown that an imaging panel (IP) near the patient can be used to determine treatment parameters such as the dwell time and source positions in a single material pelvic phantom. In this study we will use a heterogeneous head phantom to test this IP approach, and simulate common treatment errors to assess the sensitivity and specificity of the error-detecting capabilities of the IP.

METHODS AND MATERIALS: A heterogeneous head-phantom consisting of soft tissue and bone equivalent materials was 3D-printed to simulate a base of tongue treatment. An High Dose Rate treatment plan with 3 different catheters was used to simulate a treatment delivery, using dwell times ranging from 0.3 s to 4 s and inter-dwell distances of 2 mm. The IP was used to measure dwell times, positions and detect simulated errors. Measured dwell times and positions were used to calculate the delivered dose.

RESULTS: Dwell times could be determined within 0.1 s. Source positions were measured with submillimeter accuracy in the plane of the IP, and average distance accuracy of 1.7 mm in three dimensions. All simulated treatment errors (catheter swap, catheter shift, afterloader errors) were detected. Dose calculations show slightly different distributions with the measured dwell positions and dwell times (gamma pass rate for 1 mm/1% of 96.5%).

CONCLUSIONS: Using an IP, it was possible to verify the treatment in a realistic heterogeneous phantom and detect certain treatment errors.

Keywords: High dose rate brachytherapy; Treatment verification; *In vivo* dosimetry; Error detection; Dose recalculation

Introduction

High-dose-rate (HDR) brachytherapy has seen many technological developments over the last years (1), leading to very good local control rates with lower toxicity rates for cancer patients with different tumor sites (2–5). However, with these developments the complexity of the treatment increased as well, making it more prone to human error (6,7). These errors often stay unnoticed and could result in underdosing of the target volume, and overdosing in

Received 15 June 2022; received in revised form 24 October 2022; accepted 26 November 2022

Disclosures: TVW, GPF, RV, CVB, EVL, LL, BV, MB and FV were supported by research grants from KWF (Grant 12780—Bas Mulder award) and Topspecialistische Zorg en Onderzoek ZonMw ("Making radiotherapy sustainable" – project number 10070012010002). TVW, GPF, RV, CVB, EVL, LL, BV, MB, BR and FV received funds by Varian Medical Systems during the conduct of this study.

* Corresponding author: Department of Radiation Oncology (Maastro), GROW School for Oncology and Reproduction, Maastricht University Medical Centre+, Dr. Tanslaan 12, 6229 ET Maastricht, The Netherlands, Tel.: +31 88 4455666; fax: +31 88 4455667.

E-mail address: frank.verhaegen@maastro.nl (F. Verhaegen).

[#] These authors contributed equally to this manuscript.

https://doi.org/10.1016/j.brachy.2022.11.012

surrounding tissues and organs at risk. Real-time *in vivo* dosimetry (IVD) would allow for determination of the dose that was actually delivered and potential adjustment of the treatment plan if needed. The dose can be calculated post treatment, by using the measured dwell times and source positions. This method has been recommended by the ESTRO task group for *in vivo* dosimetry in brachytherapy (8). Real-time treatment verification could alert the clinical personnel during the treatment and allow them to adjust the procedure or interrupt it, provided that the uncertainty of the system is low enough (8).

Currently, there is no widespread clinical method to verify their brachytherapy treatments in real time as there are no commercially available methods. Different methods are being explored, such as internal point dose detectors (9,10) and imaging panels (IP) (11,12). The latter option uses an external IP to detect photons coming from the Iridium-192 source during the treatment. A benefit of this approach is that not just catheter movement, but also movement of the entire template or applicator can be detected, which is not possible with internal detectors that are integrated into the template or applicator. In previous work it was shown that an IP could be used to verify a prostate treatment in a single-material pelvic phantom, showing accuracy in determining dwell times within 0.1 s and reconstructing the dwell position with submillimeter accuracy (13). Although this phantom was modeled using the shape of a real human and it was possible to insert different materials and a transrectal ultrasound probe, the accuracy for different treatment sites needs to be verified if possible with even more realistic phantoms to test the approach before a future clinical trial can be started.

In this study the feasibility of using the IP to verify brachytherapy treatments was investigated by using a realistic head phantom with different materials, mimicking soft and bone-like tissues. This phantom was specifically designed for dosimetry of base in tongue brachytherapy treatments, as it has cavities fitted for brachytherapy needles below the chin. Different types of errors were simulated to test what magnitude of errors the system is able to detect. Ultimately dose calculations were performed using the measured dwell positions and times and compared to the dose distribution of the planned positions.

Methods and materials

3D printed phantom

Brachytherapy experiments with phantoms are commonly performed using homogeneous phantoms (11,14,15). Although it can be an accurate approximation depending on the measurement technique (e.g. with dosimeters close to the source), homogeneous phantoms are not ideal to evaluate IP based treatment verification due to unrealistic geometry and scattering conditions. In addition, photons leaving the patient would cross a relevant amount of tissue causing beam hardening or softening (depending on the composition) that can affect the IP response. We designed and manufactured a realistic in-house 3D printed head phantom with cavities for needle placement simulating a base of the tongue treatment.

The phantom was based on a CT scan of a PBU-60 phantom (Kyoto Kagaku, Kyoto, Japan). Patient images were not used since it would be difficult to guarantee complete anonymization while using facial reconstruction methods. The CT scan was segmented into soft and bone tissue using Hounsfield Unit (HU) thresholds and converted into a 3D model.

The phantom was manufactured using a custom-made Fused Deposition Modeling printer using two materials. PLA ($C_3H_4O_2$) was used to mimic soft tissue whilst a custom filament was used to mimic bone, hereafter referred to as bone filament. Although PLA filament with copper inclusions has been used to mimic bone tissue (16) producing similar HU values, the material composition will lead to wrong mass or electron density assignment and dosimetric properties that are essential in radiotherapy. To overcome this limitation, a custom bone filament that includes 38% of calcium carbonate ($CaC0_3$), resulting in approximately 15.2% of calcium, was developed by ColorFabb (Belfeld, the Netherlands) specifically for this project. The bone material has a mass density of approximately 1.5 g/cm^3, and a Z_{eff} of approximately 6.25.

Experimental workflow

In Fig. 1 the experimental workflow of the activities performed to realize IVD for the 3D printed phantom can be found. All data analysis was done using Matlab 2019b (Natick, MA).

In preparation for the treatment delivery, a CT acquisition of the head phantom with holder, inserted brachytherapy needles and markers had to be obtained. The CT was made using a SIEMENS SOMATOM Confidence scanner, using a slice thickness of 1 mm for the acquisition. The lead ball-shaped markers (The Suremark Company, Simi Valley) have a diameter of 2 mm and were placed on the phantom so that their projection would be visible on the IP image.

A treatment plan was created using the treatment planning system (TPS) BrachyVision (version 16, Varian Medical Systems, Palo Alto) based on CT images of the phantom. This resulted in a plan where all 3 catheters consisted of 20 dwell positions with an interdwell distance of 2 mm and a dwell time ranging from 0.3 to 4.0 seconds.

Experimental setup

The measurement itself is performed with the head phantom positioned on the treatment couch and the IP to the side of the head (Fig. 2a) or below the couch

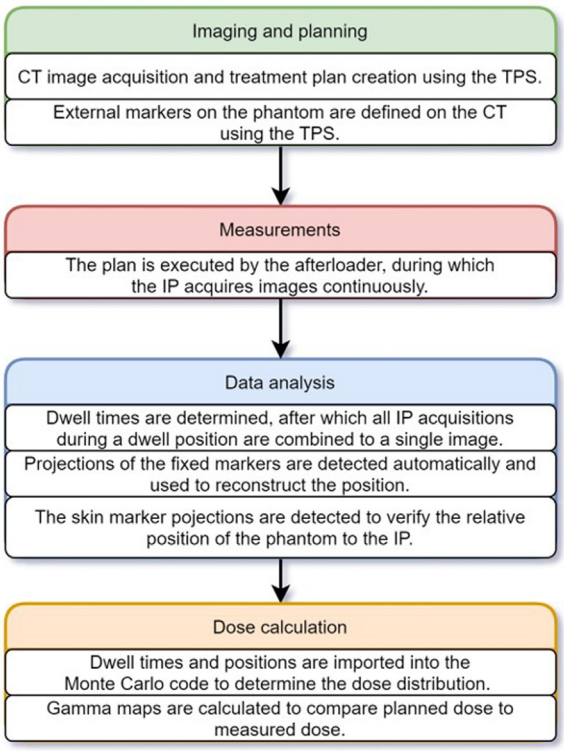

Fig. 1. Overview of the used experimental workflow to perform treatment verification in the 3D printed head phantom. (TPS = treatment planning system). (For interpretation of the references to color in this figure legend, the reader is referred to the Web version of this article.)

(Fig. 2b). The experiments were performed using a GammaMed Plus HDR 192-Ir source and GammaMed Plus iX afterloader (Varian Medical Systems). The used IP (PAXSCAN 2530HE, Varex Imaging), has a detection area of 24.5×30.2 cm^2, with 1792 by 2176 pixels and 0.139 mm resolution. As determined to be the optimal settings in previous research (13), the 2×2 pixel binning mode was used. Binning was beneficial, because it allows for a higher frame rate (10 fps), requires less storage data, and the full image resolution is unnecessarily high for our purposes, for which 0.28 mm suffices. The intended position of the IP will be either on the lateral side of the patient, or below the treatment table (see Fig. 2b). Due to the fact that the table will attenuate gamma rays coming from the ^{192}Ir source, its effect on the IP acquisitions had to be investigated. The distance of the surface of the phantom to the patient was set at 25 cm.

Treatment verification

After the measurement, dwell times were determined by the IrIS (Iridium Imaging System) software, which detects when the source is moving or at rest by comparing the pixel intensities in consecutive acquisitions (13). All periods where the source was at rest for multiple time frames were considered dwell positions. Subsequently all frames of a single dwell position were combined to obtain a single combined image for every dwell position (Fig. 3b).

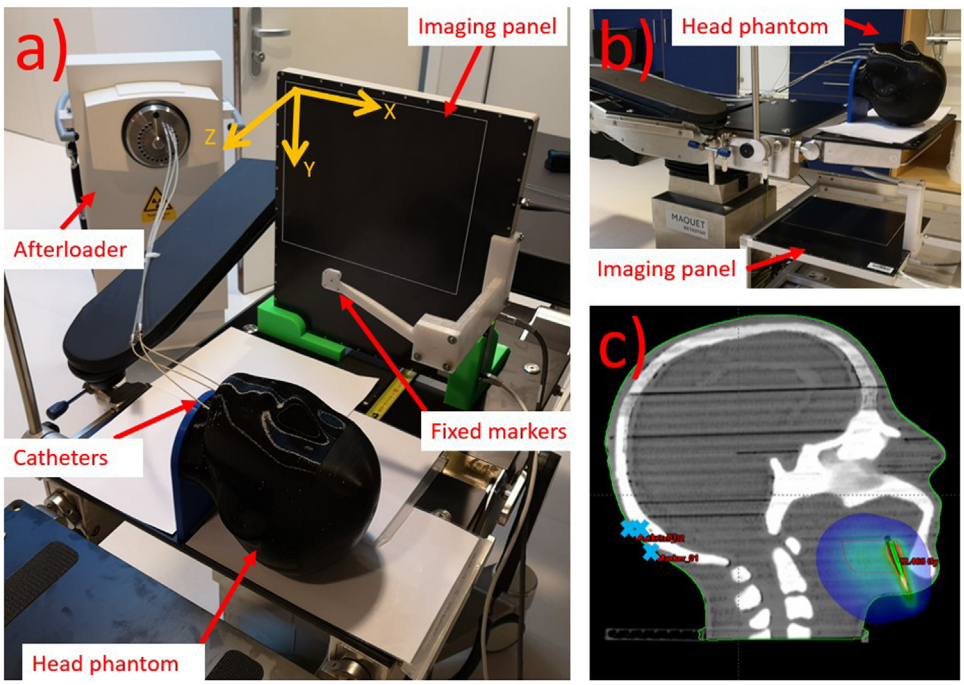

Fig. 2. Overview of the experimental setup. Figure (a) shows the experimental setup where the IP is positioned to the side of the patient. The distance between phantom and panel has been slightly increased in this image for a better view. In yellow the coordinate system used to define dwell positions is visualized. Figure (b) is the experimental setup where the IP is located below the treatment table, and figure (c) shows a CT image of the head phantom in BrachyVision. The markers are visible in the back of the head, indicated by the cyan crosses. (For interpretation of the references to color in this figure legend, the reader is referred to the Web version of this article.)

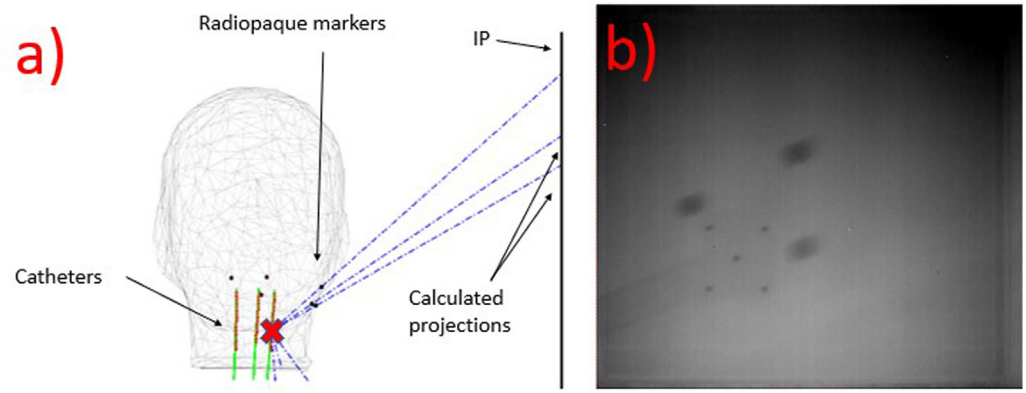

Fig. 3. (a) shows how the radiopaque markers on the surface are used to register the position of the phantom relative to the IP. The surface markers are projected on the panel, and using calculated predicted projections the position of the phantom during the measurement can be reconstructed. Source position is marked with a red cross. (b) is an example of an image acquisition, with the projections of the radiopaque markers visible (three large markers are phantom surface markers, the five smaller ones are the fixed markers). (For interpretation of the references to color in this figure legend, the reader is referred to the Web version of this article.)

In each combined image the radiopaque markers could be detected automatically. The markers on the surface of the phantom could be used to determine the position of the IP in the coordinate space of the CT image by comparing them with the calculated positions. The positions of the markers and the patient contours were imported into Matlab from the TPS, to simulate where the markers would seem for each dwell position (Fig. 3a). Using these predicted projections, the position of the IP could be approximated. The optimal position of the fiducial markers depends on the patient geometry and the relative positions of the catheters and the panel. In this case it was determined by trying to find positions where they would be projected on the panel for the maximum number of dwell positions.

A second set of markers was integrated in a 3D printed holder that was fixed on the panel to determine the position of the source (Fig. 2a). Their exact position relative to the panel is known, and therefore the projections of these markers can be used to reconstruct the source position. The same approach was used in previous research (13). Both sets of markers can be distinguished on the panel as due to magnification, the surface markers show larger projections on the panel compared to the fixed markers.

Simulated errors

Besides the plan obtained from the TPS, slightly modified plans were delivered as well to simulate potential errors that could occur during a brachytherapy treatment. Tanderup *et al*., defined a list of possible treatment errors that could occur during a brachytherapy treatment, and how relevant IVD could be in detection (6). The following errors with a major relevance for IVD were simulated:

- Wrong dwell time: due to a malfunctioning afterloader, or a software error when importing from the TPS, a dwell time is longer or shorter than planned. This error was simulated by manually adjusting the dwell time in the afterloader.
- Skipped dwell position: single or multiple dwell positions in a single catheter are skipped. This error could be detected when looking at the dwell times, as there will be less dwell positions detected than would be expected from the plan. This was simulated by setting the dwell time of some dwell positions to 0 s.
- catheter movement: the catheter is not in the same position as it was during planning. This can occur when the catheter is pulled out a few millimetres by patient movement, or by a displacement caused by internal motion, if the position of the catheter changes relative to the surrounding organs. The first scenario was simulated by doing a series of measurements while increasing the "offset" of the afterloader and keeping the catheter in the same position, thus effectively shifting all dwell positions by this offset. Internal motion was not simulated due to the phantom being solid.
- Interchanged guide tubes: this type of error can only be determined by reconstructing the source position, as the dwell times will not be altered. This error can be simulated by manually switching two catheters.

The sensitivity that is required for each error type was estimated in Table 1.

Dose calculation

The difference in dose between the planned and delivered dose was calculated using Monte Carlo simulations in MCNP6 version 1.0 (17). MCNP was used because it allows for more straightforward implementation of the measured dwell times and source positions, as it is quite difficult to import altered plans into our clinical TPS system. The created plan and CT were imported in AMIGOBrachy (18) where input files were generated, using HU threshold-

Table 1
different treatment error types with the estimated sensitivity required to detect them and the detection method.

Error type	Estimated required sensitivity	Detection method
Wrong dwell time	<0.1 s	Comparing intensity values
Skipped dwell position	<1 mm (depends on interdwell distance)	Source position reconstruction and dwell time measurement
Catheter movement	<1−5 mm (depends on clinical relevance, for example surrounding organs)	Source position reconstruction
Interchanged guide tubes	<1−5 mm (depends on distance between catheters)	Source position reconstruction

Table 2
Average displacement of all dwell positions found split by dimension and the total displacement.

Measurement	X (mm)	Y (mm)	Z (mm)	Total (mm)
No offset	0.0 ± 0.6	0.0 ± 0.8	0.0 ± 1.7	1.7 ± 0.8
Offset 1 mm	1.0 ± 0.6	0.6 ± 0.7	-0.6 ± 1.3	1.8 ± 0.8
Offset 2 mm	2.0 ± 0.6	0.7 ± 0.7	-0.1 ± 1.6	2.6 ± 0.9
Offset 3 mm	2.9 ± 0.5	1.0 ± 0.7	-0.1 ± 1.4	3.3 ± 0.7
Offset 4 mm	3.8 ± 0.6	1.1 ± 0.9	0.3 ± 1.8	4.4 ± 0.8

ing to convert the CT image into materials with different densities and compositions. The dose was recalculated using the coordinates and dwell times that were measured, to verify the impact on the dose. Both the plan with original dwell positions, and the plan with the measured positions were simulated with MCNP using the same settings for all calculations (10^{10} particles), only adjusting the positions of the dwells.

Results

3D printed phantom

The printed phantom was evaluated by a uniformity analysis of the CT scan (120 kV). There are some air gap artefacts caused by the layered printing (visible in Fig. 2c) affecting mostly the soft tissue region that was printed with a larger nozzle and lower resolution than the bone filament region to minimize printing time. The soft tissue had a mean HU value of 107 ± 51, and the bone mimicking material had a HU of 622 ± 135.

Dwell time measurements

The dwell times were measured for all catheters and dwell positions by comparing the change in total intensity values between consecutive acquisitions. Results can be found in Fig. 4. The average absolute difference for all dwell positions combined between the planned and detected dwell times was 0.002 ± 0.013 s when measured from below the table, and 0.007±0.025s when measured from the side. A paired sample t-test was performed on the measured dwell times below and beside the head phantom, which showed that there was no statistically significant dif-

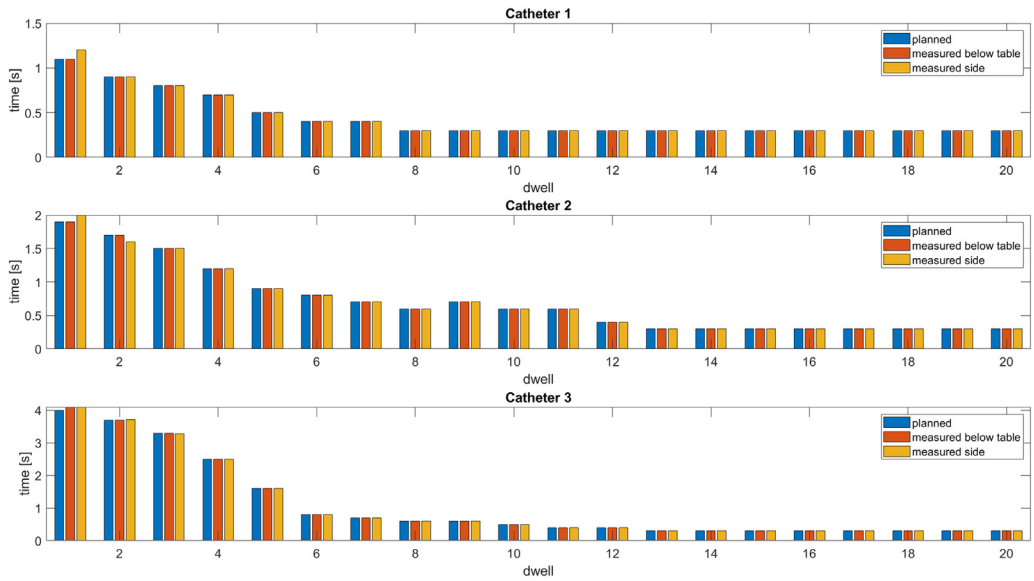

Fig. 4. Overview of the dwell times with planned dwell times (blue), measured dwell times with the IP below the table (red) and with the IP on the side of the patient (yellow). (For interpretation of the references to color in this figure legend, the reader is referred to the Web version of this article.)

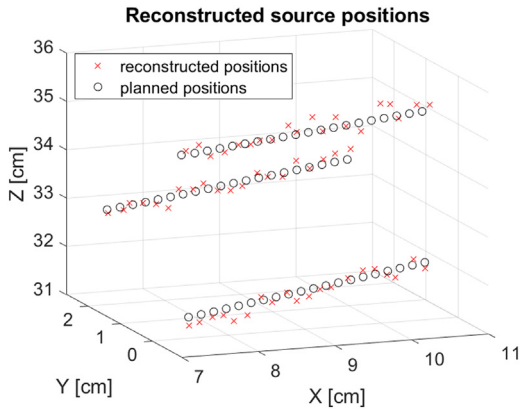

Fig. 5. Reconstructed source positions of the three catheters. The panel is positioned in the XY-plane on the side of the patient, so the Z-axis represents the distance from the panel. (For interpretation of the references to color in this figure legend, the reader is referred to the Web version of this article.)

ference between the two (p-value of 0.57). The biggest deviations are observed in the first and last dwell positions (up to 0.1 s).

Dwell positions

The source position during every dwell position was reconstructed using the detected positions of the fixed marker projections, with the panel located to the side of the patient. In Fig. 5 an overview of source reconstruction for the original plan can be found compared to the planned positions. The mean difference (and one standard deviation) between the planned and reconstructed source positions for all three catheters is 0.5 ± 0.3 mm in the X dimension, 0.7 ± 0.4 mm in the Y dimension and 1.4 ± 0.9 mm in the Z dimension. Combined this gives a total average error of 1.7 ± 0.8 mm. These values include systematic errors from the registration method, and movement of the catheter between imaging and measurement. This error can be reduced by registering the found dwell positions to the planned positions, yielding a value that is more representative of the errors caused predominately by the position reconstruction method that was implemented. This leads to a slightly higher accuracy, 0.2 ± 0.1 mm for X, 0.6 ± 0.4 mm for Y and 1.2 ± 0.8 mm in the Z dimension, and gives a combined average error of 1.4 ± 0.8 mm.

In Fig. 6 boxplots of the difference between the planned and measured positions can be found for all three dimensions. Due to the orientation of the catheter and positioning of the phantom compared to the panel, increasing the offset will move the dwell positions predominantly in the X dimension, and also somewhat in the Y dimension. This can be seen in Fig. 5, where the average position of all measured dwells compared to the planned dwells is shown for the different offsets that were introduced. The predicted average change in position is shown with a black cross as a comparison, which was approximately 0.94 mm in X, 0.32 mm in Y and 0.06 mm in Z for every mm offset.Table 2 shows the displacement for all dimensions, and it can be noted that the standard deviation of the Z coordinates found where much higher than those in X and Y.

Dose calculations

The calculated dose with the planned dwell positions was compared to the recalculated dose based on the measured dwell positions. Both dose distributions were obtained from Monte Carlo simulations. In Fig. 7 the dose distributions are visualized with isodose lines, superimposed over the planning CT image.

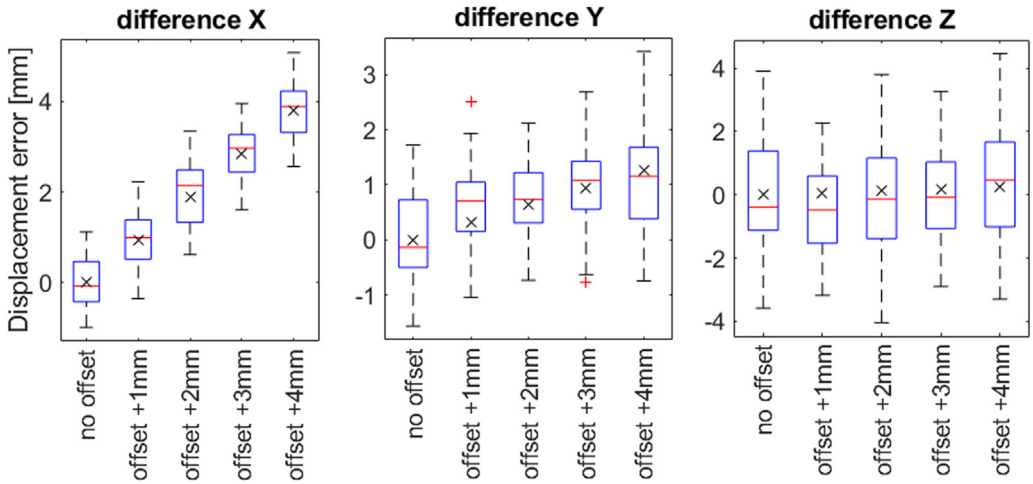

Fig. 6. Distribution of the difference per dimension between the reconstructed source positions and the planned positions. The offset of the source was increased from 0 to 4 mm. The black crosses indicate the expected movement based on the catheter orientations. (For interpretation of the references to color in this figure legend, the reader is referred to the Web version of this article.)

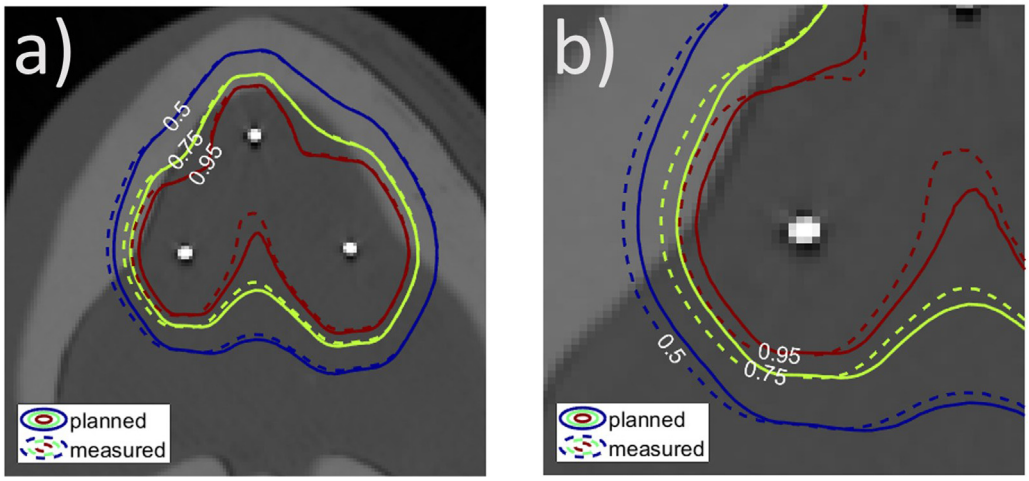

Fig. 7. Isodose lines of the dose distributions calculated with MCNP. The solid line shows the dose distribution when the planned dwell position and times are used as input, the dashed lines shows the isodoses when calculated with the reconstructed positions and times. (a) shows an overview of all three catheters, (b) is zoomed in on a single catheter to better show the difference between the isodoses. (For interpretation of the references to color in this figure legend, the reader is referred to the Web version of this article.)

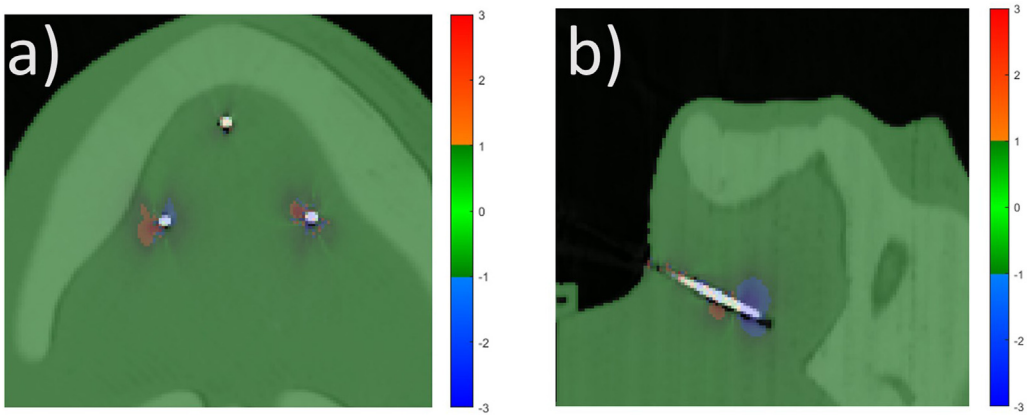

Fig. 8. Gamma maps showing the voxels that pass the dose difference and distance to agreement criteria (green) and do not pass (red/blue). (a) gamma map of the measured dose (no offset) compared to the planned dose, using a gamma criterion of 1mm/1%. (b) gamma map with a criterion of 1 mm/1% comparing the offset of 4 mm to the planned positions in the sagittal plane to show the effect of this introduced offset. (For interpretation of the references to color in this figure legend, the reader is referred to the Web version of this article.)

The dose can be compared using a gamma analysis, see Fig. 8. A strict gamma criterion of 1mm/1% leads to a gamma passing rate of 86.6% in the "tumor area," which was defined as the area where the planned dose was 95% of the prescribed dose or higher. If we take a larger area of interest, for example, where the dose is higher than 50% of the prescribed dose, the pass rate increases to 95.9%, as the failing voxels are all close to the catheter. Table 3 shows the pass rates for more lenient gamma criteria.

The dose of the offset cases that simulate the catheter moving out of the patient was also calculated, and the passing rates can be found in Table 3. The passing rate goes down when the offset increases.

Discussion

In this work it was shown that dwell times and source positions of a brachytherapy treatment in a static head phantom can be verified using an IP. Additionally, several common treatment errors were simulated and these could be detected by the system.

Even though the phantom used in this study is an improvement on those used in earlier studies due to its realistic geometry and use of different materials, it has to be acknowledged that the densities and corresponding HU values of the phantom can still be improved upon. Ideally the density of the bone structures in the phantom would have been lower; however it is difficult to find filaments and

Table 3
Pass rates of different measurements and gamma criteria, where the dose calculated with the planned positions is compared to the dose calculated with the measured positions

Gamma crit.	Pass rate (dose >50% prescribed)			Pass rate (dose >95% prescribed)		
	1 mm/1%	1 mm/3%	1 mm/10%	1 mm/1%	1 mm/3%	1 mm/10%
No offset	95.9%	98.9%	99.8%	86.6%	95.6%	99.1%
Offset 1 mm	94.4%	98.6%	99.8%	82.4%	95.0%	99.2%
Offset 2 mm	93.2%	98.4%	99.7%	77.2%	93.5%	99.0%
Offset 3 mm	91.2%	97.8%	99.6%	71.2%	91.7%	98.6%
Offset 4 mm	82.9%	95.1%	99.2%	58.3%	83.7%	97.0%

printing settings that precisely match human tissue properties.

The dwell time could be determined within 0.002s with a frame rate of 10 fps. This margin of error was much lower than the smallest dwell time error that was possible to simulate (0.1 s), so all dwell time errors could be detected. The relatively high error for the first dwell could be caused by the different approach used by the afterloader to determine the dwell time for the first dwell position (19). Higher frame acquisition rates could yield better results, but also rapidly increases the amount of data generated. The higher attenuation caused by the table did not cause significantly worse results in determining the dwell time.

Dwell positions can be reconstructed with an accuracy of 1.7 mm, of which 1.4 mm can entirely be attributed on the uncertainty of the reconstruction method. With this uncertainty it was difficult to distinguish between two dwell positions that are next to each other, as the inter dwell distance was 2 mm. However, errors with bigger magnitudes can easily be detected, so it was possible to find swapped catheters. Most of the uncertainty in 3D reconstruction can be attributed to the "Z dimension," which represents the distance from the panel. Misdetection of the marker projections by a small margin has a larger effect on the prediction of the Z coordinate of the source, as a result of the design of the holder. The clinical relevance of these uncertainties is hard to determine, since it depends on the relative position of a dwell position compared to the target volume and organs at risk. This is something that should be examined in future work. Possibly a holder with increased distance between the markers would yield more accurate results in this dimension and allow for more accurate source tracking, or even a second orthogonally placed panel could be used. A panel with a higher resolution could improve the accuracy of the source reconstruction, and a larger field of view would allow for improved positioning of the radiopaque markers. Higher density markers should be investigated as they could allow for more accurate source tracking.

The surface marker registration method to determine the location of the phantom compared to the panel also contributes to the uncertainty of the reconstruction method. Registering the measured set of source positions on the planned positions can be used to reduce this effect, but this only works for a static phantom because a patient can move during the treatment. A method to increase the accuracy could be the use of a surface scanning system that tracks the external motion of the patient, comparable to methods that are already being used to track patients during external beam therapy (20). To account for internal motion other solutions could be implemented, for example by extracting anatomical information from the panel acquisitions (21).

Previous results with a pelvic phantom mimicking a prostate treatment showed similar results in dwell times, but slightly higher accuracy in determining the dwell position (13). Where for the pelvic phantom a submillimeter accuracy was reported, for the head phantom this was up to 1.4 mm when the systematic error was removed. The slightly worse results for the head phantom could be explained by the bone material or the different shape of the phantom, as the distance between the source and the sets of markers is different. Another difference is that the pelvic phantom could be positioned in a rigidly fixed location to the panel using the holder, which allows for more accurate positioning of the experimental setup. It shows that more extensive research with different phantoms, setups, and types of markers has to be performed to determine the effectiveness for different treatment sites. Additionally, tests with moving phantoms (for example by using motion platforms) should be performed to verify the effectiveness in dynamic cases.

An additional source of dwell position uncertainty that can occur during brachytherapy treatments is needle migration between treatment planning and the treatment itself (6). Previous research suggests that catheter migration of more than 3 mm is dosimetrically relevant enough to make a new dose plan in HDR brachytherapy treatment for prostate cases (22,23), and a threshold of 2 mm should be used in cases when dose levels are over 15 Gy (24). Naturally these threshold values will differ for other treatment sites, depending on the surrounding organs at risk, but these could be used as a general estimation of the precision needed. In general, our method would be able to determine if a catheter is shifted by 1 mm, as shown by increasing the offset (Fig. 6), if this shift is in the X−Y plane. The higher uncertainty of the Z dimension

makes that only shifts of 2 mm or larger can reliably be detected.

Alternatively, catheter reconstruction could be performed before the treatment using an extra in-room imaging device, such as a ceiling mounted X-ray system (25), or using electromagnetic tracking (26). These methods have submillimeter accuracy, but are only used to verify the catheter position before the treatment and not during treatment. Furthermore, the X-ray systems expose the patient to additional imaging dose, and the electromagnetic tracking requires more advanced equipment. Possibly, a combination of pretreatment imaging, source tracking during treatment and tracking the motion of the patient could be a promising approach for the most accurate brachytherapy treatment verification.

As demonstrated, the actual delivered dose can be recalculated using the obtained dwell positions and reconstructed catheter position during treatment for the different scenarios. Comparing the planned and measured dose distributions and gamma maps show that there is a difference in around the catheters, caused by the uncertainty of the source tracking method. However, since the pass rate seems to go down somewhat proportionate to the magnitude of the error that was introduced to the plan, there could still be information derived from these dose calculations related to the effectiveness of the treatment.

More research is needed to determine the effect of other treatment errors on the patient. Nunez *et al*. already showed how the effect of treatment errors in prostate cases can be quantified by simulating them (27), but this is also needed for other treatment sites as it shows how relevant it is to perform *in vivo* dosimetry in brachytherapy.

Conclusion

It was demonstrated with a realistic 3D printed phantom that it should be possible to perform treatment verification for head and neck cases in brachytherapy using an IP. Dwell time errors of 0.1s can be detected, and the source position can be reconstructed with an accuracy of <1.7 mm, under optimal conditions. This allows for the detection of several commonly occurring treatment errors, including wrong dwell times, a moving catheter or swapped catheters. Using the measured treatment parameters, it is shown that the dose can be recalculated and compared to the planned dose, which allows for post treatment analysis and adaptation of possible future fractions.

Acknowledgments

We thank Dr. Murillo Bellezzo for his help with the measurements, and Dr. Mark Podesta for his helpful Matlab functions.

References

[1] Cunha JAM, Flynn R, Bélanger C, et al. Brachytherapy future directions. *Semin Radiat Oncol* 2020;30:94–106. doi:10.1016/j.semradonc.2019.09.001.

[2] Sturdza A, Pötter R, Fokdal LU, et al. Image guided brachytherapy in locally advanced cervical cancer: improved pelvic control and survival in RetroEMBRACE, a multicenter cohort study. *Radiother Oncol* 2016;120:428–433. doi:10.1016/j.radonc.2016.03.011.

[3] Crook J, Marbán M, Batchelar D. HDR prostate brachytherapy. *Semin Radiat Oncol* 2020;30:49–60. doi:10.1016/j.semradonc.2019.08.003.

[4] Westerveld H, Schmid M, Nout R, et al. Image-Guided Adaptive Brachytherapy (IGABT) for primary vaginal cancer: results of the international multicenter RetroEMBRAVE cohort study. *Cancers (Basel)* 2021;13:1459. doi:10.3390/cancers13061459.

[5] Venkat P, Han J, Demanes DJ. Brachytherapy of the head and neck: an University of California Los Angeles guide to morbidity reduction. *Brachytherapy* 2021;20:1014–1040. doi:10.1016/j.brachy.2020.12.002.

[6] Tanderup K, Beddar S, Andersen CE, et al. In vivo dosimetry in brachytherapy. *Med Phys* 2013;40:070902. doi:10.1118/1.4810943.

[7] Kertzscher G, Rosenfeld A, Beddar S. In vivo dosimetry: trends and prospects for brachytherapy. *Br J Radiol* 2014;87:20140206. doi:10.1259/bjr.20140206.

[8] Fonseca GP, Johansen JG, Smith RL, et al. In vivo dosimetry in brachytherapy: requirements and future directions for research, development, and clinical practice. *Phys Imaging Radiat Oncol* 2020;16:1–11. doi:10.1016/j.phro.2020.09.002.

[9] Linares Rosales HM, Duguay-Drouin P, Archambault L. Optimization of a multipoint plastic scintillator dosimeter for high dose rate brachytherapy. *Med Phys* 2019;46:2412–2421. doi:10.1002/mp.13498.

[10] Jørgensen EB, Kertzscher G, Buus S, et al. Accuracy of an in vivo dosimetry-based source tracking method for afterloading brachytherapy — a phantom study. *Med Phys* 2021;48:2614–2623. doi:10.1002/mp.14812.

[11] Fonseca GP, Podesta M, Bellezzo M, et al. Online pretreatment verification of high-dose rate brachytherapy using an imaging panel. *Phys Med Biol* 2017;62:5440–5461. doi:10.1088/1361-6560/aa7028.

[12] Smith RL, Hanlon M, Panettieri V, et al. An integrated system for clinical treatment verification of HDR prostate brachytherapy combining source tracking with pretreatment imaging. *Brachytherapy* 2018;17:111–121. doi:10.1016/j.brachy.2017.08.004.

[13] Fonseca GP, van Wagenberg T, Voncken R, et al. Brachytherapy treatment verification using gamma radiation from the internal treatment source combined with an imaging panel — a phantom study. *Phys Med Biol* 2021;66. doi:10.1088/1361-6560/abf605.

[14] Smith RL, Taylor ML, McDermott LN. Source position verification and dosimetry in HDR brachytherapy using an EPID. *Med Phys* 2013;40:1–12. doi:10.1118/1.4823758.

[15] Watanabe Y, Muraishi H, Takei H, et al. Automated source tracking with a pinhole imaging system during high-dose-rate brachytherapy treatment. *Phys Med Biol* 2018;63. doi:10.1088/1361-6560/aacdc9.

[16] Savi M, Andrade MAB, Potiens MPA. Commercial filament testing for use in 3D printed phantoms. *Radiat Phys Chem* 2020;174:108906. doi:10.1016/j.radphyschem.2020.108906.

[17] Goorley T, James M, Booth T, et al. Initial MCNP6 Release Overview. *Nucl Technol* 2012;180:298–315. doi:10.13182/NT11-135.

[18] Fonseca GP, Reniers B, Landry G, et al. A medical image-based graphical platform-Features, applications and relevance for brachytherapy. *Brachytherapy* 2014;13:632–639. doi:10.1016/j.brachy.2014.07.004.

[19] Bellezzo M, Baeza JA, Voncken R. Mechanical evaluation of the

Bravos afterloader system for HDR brachytherapy. *Brachytherapy* 2019;18:852–862. doi:10.1016/j.brachy.2019.06.005.

[20] Freislederer P, Kügele M, Öllers M, et al. Recent advances in surface guided radiation therapy. *Radiat Oncol* 2020;15:187. doi:10.1186/s13014-020-01629-w.

[21] van Wagenberg T, Paiva Fonseca G, Verhaegen F. OC-0045 extracting anatomical information from Iridium-192 gamma images using artificial intelligence. *Radiother Oncol* 2021;158:S33–S34. doi:10.1016/s0167-8140(21)06287-3.

[22] Aluwini S, Busser WMH, Baartman LEA, et al. Fractionated high-dose-rate brachytherapy as monotherapy in prostate cancer: does implant displacement and its correction influence acute and late toxicity? *Brachytherapy* 2016;15:707–713. doi:10.1016/j.brachy.2016.05.008.

[23] Mason J, Henry A, Bownes P. Error detection thresholds for routine real time in vivo dosimetry in HDR prostate brachytherapy. *Radiother Oncol* 2020;149:38–43. doi:10.1016/j.radonc.2020.04.058.

[24] Buus S, Lizondo M, Hokland SB, et al. Needle migration and dosimetric impact in high-dose-rate brachytherapy for prostate cancer evaluated by repeated MRI. *Brachytherapy* 2018;17:50–58. doi:10.1016/j.brachy.2017.08.005.

[25] Smith RL, Haworth A, Panettieri V. 3D catheter reconstruction in HDR prostate brachytherapy for pre-treatment verification using a flat panel detector. *Phys Medica* 2017;39:121–131. doi:10.1016/j.ejmp.2017.06.008.

[26] Tho D, Lavallée MC, Beaulieu L. Performance of an enhanced afterloader with electromagnetic tracking capabilities for channel reconstruction and error detection. *Med Phys* 2021;48:4402–4410. doi:10.1002/mp.14877.

[27] Nunez DA, Trager M, Beaudry J, et al. Quantifying clinical severity of physics errors in high-dose rate prostate brachytherapy using simulations. *Brachytherapy* 2021;20:1062–1069. doi:10.1016/j.brachy.2021.05.007.